Lessened projections of Arctic warming and wetting after correcting for model errors in global warming and sea ice cover

CLIMATOLOGY

Lessened projections of Arctic warming and wetting after correcting for model errors in global warming and sea ice cover

Ziyi Cai[1,2], Qinglong You[1]*, James A. Screen[2], Hans W. Chen[3], Ruonan Zhang[1], Zhiyan Zuo[1], Deliang Chen[4,5], Judah Cohen[6,7], Shichang Kang[8], Renhe Zhang[1]

Credible projections of Arctic warming and wetting (AWW) are essential for informed decision-making in a changing climate. However, current AWW projections from state-of-the-art climate models carry uncertainties. Using observational datasets and CMIP6 model simulations, we demonstrate that the observed historical global warming trend and the climatological mean pattern of Arctic sea ice can serve as effective constraints on AWW projections. Under SSP2-4.5, the constrained warming by the end of the century is reduced from 5.5° to 4.6°C. Similarly, the projected wetting decreases from 6.8 to 5.7 millimeter per month. The inter-model spread in warming and wetting is reduced by 25 and 15%, respectively. The reduction is the largest in the Barents-Kara seas, reducing warming by 1.2°C, lessening wetting by 1.7 millimeter per month, and decreasing the inter-model spread by one-third. Our findings suggest that unconstrained CMIP6 projections overestimate future AWW, particularly in the Barents-Kara seas, due to an overestimation of historical global warming and excessive sea ice in the models.

INTRODUCTION

A notable feature of observed climate change is the greater increase in temperature and precipitation in the Arctic compared to the global average, known as Arctic warming and wetting (AWW) amplification (*1*–*4*). This amplification has profound implications for the climate system (*5*), such as accelerating the retreat of Arctic sea ice (*6*), promoting mass loss from the Greenland ice sheet (*7*), and triggering permafrost thaw (*8*). Future AWW amplification is expected to intensify further changes in the Arctic water cycle (*9*), increase river discharge, and disturb the freshwater balance in the ocean, posing substantial risks to Arctic ecosystems and environments (*10*). In addition, although still debated, several studies suggest that Arctic warming may intensify extreme climate events in the northern midlatitudes (*11*–*13*). Accurate and reliable projections of AWW changes are therefore critical for planning adaptation and mitigation strategies in a rapidly changing climate.

Most projections of future climate change rely on the Coupled Model Intercomparison Project (CMIP). While models from CMIP phases 3 to 6 have steadily improved in representing key climate elements in the Arctic (*4*, *14*–*16*), many CMIP5 and CMIP6 models still fail to accurately capture the sensitivity of Arctic sea ice loss to global warming (*16*, *17*). The multi-model ensemble means (MMEMs) of CMIP5 and CMIP6 overestimate the mean state of Arctic sea ice while underestimating its reduction (*18*) and also underestimate Arctic mean temperatures (*14*, *15*) and precipitations over the Arctic Ocean (*2*), particularly during the cold season. Model uncertainty remains high in the Arctic, especially in the boundary regions between sea ice and open ocean (*19*). Efforts to reduce AWW projection uncertainty have included using MMEMs to mitigate internal variability among models (*14*, *20*), reweighting projections based on agreement with observations (*2*, *21*), and using linear regression methods for more robust future projections (*22*). However, these methods do not fully eliminate biases or errors in model simulations as many models share similar biases (*15*).

A more effective approach for reducing uncertainties in multi-model results is the emergent constraint method (*23*–*25*), which has gained traction in recent years, particularly for Arctic issues of concern to the public and policymakers. These issues include projections of an ice-free Arctic, changes in the Greenland Ice Sheet (*26*–*28*), and temperature changes (*29*, *30*). The emergent constraint method establishes a relationship with a solid physical basis between current observations (predictor) and future climate change (predictand) across climate models. The observed predictor value is then used to adjust the simulated predictand (*24*). Recent studies indicate that some CMIP6 models exhibit excessive equilibrium climate sensitivity (ECS), leading to an overestimation of historical and future global warming (*31*, *32*), suggesting potential biases in other model outputs as well (*32*). By using historical global temperature and precipitation trends to constrain future projections, the median global warming under a high-emission scenario drops from 4.01° to 3.44°C by the end of the century (*33*). The upper limit of the median global precipitation increase under a moderate emission scenario can be lowered from 6.2 to 5.2 to 5.7% (*34*). Similar methods applied to regional projections have shown that unconstrained models overestimate warming and water cycle intensification in regions such as Asia (*35*), Africa (*36*), and the Arctic (*29*). A recent study further reduced uncertainty in regional climate projections by correcting precipitation changes across various regions based on historical warming trends in multiple models (*37*). These findings have inspired the use of historical global warming to constrain future Arctic wetting, as

[1]Department of Atmospheric and Oceanic Sciences & Institute of Atmospheric Sciences & Key Laboratory of Polar Atmosphere-Ocean-Ice System for Weather and Climate, Ministry of Education, Fudan University, 200438 Shanghai, China. [2]Department of Mathematics and Statistics, University of Exeter, Exeter, UK. [3]Department of Space, Earth and Environment, Chalmers University of Technology, SE-412 96 Gothenburg, Sweden. [4]Department of Earth System Sciences, Tsinghua University, Beijing 100084, China. [5]Department of Earth Sciences, University of Gothenburg, S-405 30 Gothenburg, Sweden. [6]Atmospheric and Environmental Research Inc., Lexington, MA, USA. [7]Department of Civil and Environmental Engineering, Massachusetts Institute of Technology, Cambridge, MA, USA. [8]Key Laboratory of Cryospheric Sciences and Frozen Soil Engineering, Northwest Institute of Eco-Environment and Resources, Chinese Academy of Sciences, Lanzhou 730000, China.
*Corresponding author. Email: qlyou@fudan.edu.cn

models that overestimate historical warming tend to overestimate future warming and its associated increase in precipitation (*33*, *37*). Moreover, using the global warming trend accounts for both local and nonlocal processes that affect AWW (*19*). Considering the limitations of data quality, temperature records are generally more reliable than precipitation indicators (*38*).

However, most previous studies focus on regional average changes, neglecting spatial information. Because of the influence of underlying sea ice, there is spatial variability in the magnitude of future AWW as well as in model uncertainties (*4*, *39*). The reduction of uncertainty through emergent constraints may also vary geographically. In this study, we combine historical global warming trends with spatial patterns of historical sea ice concentration (SIC) to constrain both the mean changes and spatial patterns of future AWW. Our results not only reduce uncertainties in Arctic-mean AWW projections but also constrain the spatial patterns of projected changes. Moreover, we found that the SIC constraint did not change the Arctic average results much but altered the spatial distribution of AWW, especially leading to further downward adjustments in AWW projections for some Arctic subregions. These findings could provide valuable insights for scientific research and socioeconomic planning for climate change adaptation.

RESULTS

Projected AWW in the CMIP6 models

We begin by examining the projected AWW under three emission scenarios from CMIP6 models (table S1) before applying emergent constraints. Previous studies comparing reanalysis datasets with station observations (fig. S1) have shown that the European Centre for Medium-Range Weather Forecasts Reanalysis v5 (ERA5) dataset outperforms others in accurately capturing AWW (*2*, *4*, *14*). Thus, we used ERA5 as the reference field in this study. As illustrated in Fig. 1, the MMEM generally simulates the AWW changes seen in ERA5 during the period 1960–2014, with the rate of increase notably higher in the Arctic than the global average. In all emission scenarios, future AWW amplification continues to intensify. By the end of this century, under the socioeconomic pathway (SSP) 1-2.6, SSP2-4.5, and SSP5-8.5 scenarios, the projected Arctic average warming (17 to 83% likely range) relative to 1995 to 2014 is 3.4°C (1.8° to 5.4°C), 5.5°C (3.8° to 7.4°C), and 9.6°C (7.0° to 12.0°C), respectively. Correspondingly, the projected Arctic-mean wetting is 4.4 mm/month (2.2 to 6.5 mm/month), 6.8 mm/month (4.3 to 9.3 mm/month), and 12.4 mm/month (8.8 to 16.0 mm/month), respectively.

Under the low to moderate emission scenarios, AWW amplification primarily occurs in the northern Barents-Kara seas, whereas under the high-emission scenario, the maximum values are distributed across the entire Arctic Ocean. The spatial pattern of wetting is somewhat coherent with the warming, indicating that thermal effects are more pronounced than dynamic effects in driving future wetting (*40*). In addition, the spatial pattern of local sensitivity (see Materials and Methods) to AWW is largely consistent with the spatial pattern of AWW changes, suggesting that local processes play a dominant role in shaping future AWW changes (*39*, *41*). Furthermore, CMIP6 models exhibit a wide inter-model spread in AWW,

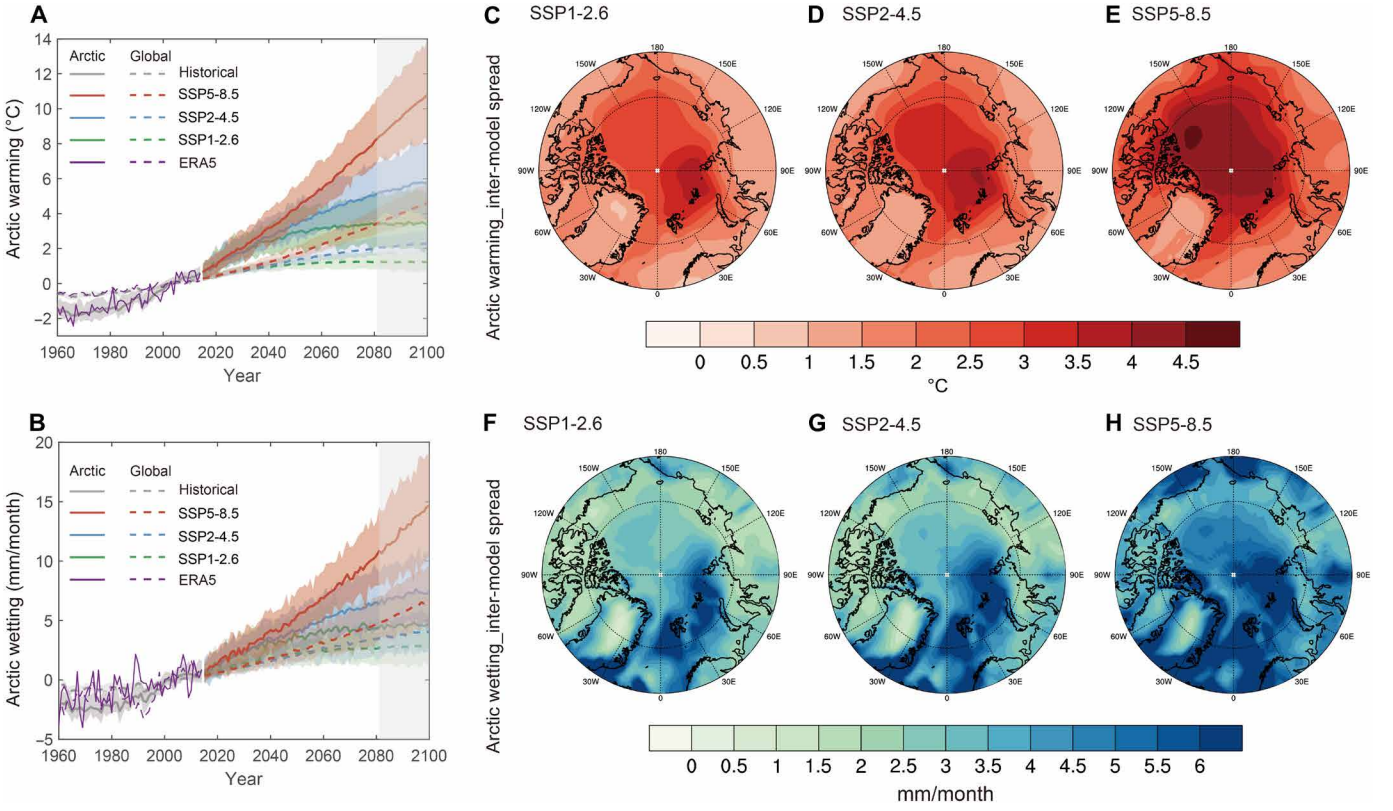

Fig. 1. Original CMIP6-projected results. Time series of Arctic (solid lines) and global (dotted lines) annual (**A**) near-surface temperature and (**B**) precipitation anomalies from 1960 to 2100. For each scenario, the median (solid lines) and the 17 to 83% likely range (shading) are shown. (**C** to **H**) Inter-model spread (83% threshold minus 17% threshold) of spatial patterns of AWW under the SSP1-2.6, SSP2-4.5, and SSP5-8.5 scenarios by the end of this century.

both in historical simulations and future projections (Fig. 1). The regions with the largest inter-model spread extend from the Barents-Kara seas to the central Arctic Ocean.

The linkage between historical global warming and future AWW

To reduce the uncertainty in AWW projections from CMIP6 models, it is essential to identify the dominant factors contributing to the inter-model spread, providing a physical basis for building emergent constraint relationships. Previous studies (*29*, *37*) suggest that a feasible approach to constraining future AWW involves aligning model-simulated global warming with observations. Figure 2 (A and B) shows the cross-model correlation coefficients (r) between the multimodels projected AWW at the end of this century under the SSP5-8.5 scenario and simulated global warming trends in historical runs based on multiple observational datasets. We calculated the relationship between historical global warming trends over different time spans and future AWW, revealing a strong correlation between future AWW and simulated long-term historical global warming ($r = 0.64$ and 0.66, respectively, $P < 0.05$).

The physical basis for this relationship lies in the fact that both historical and future changes in global warming are primarily driven by rising CO_2 concentrations, and the response to cumulative CO_2 increases is approximately linear (*42*). Arctic mean temperature changes are closely correlated with global mean temperature, both historically ($r = 0.89$, $P < 0.05$) and in future scenarios ($r = 0.89/0.89/0.93$ for SSP1-2.6/SSP2-4.5/SSP5-8.5, $P < 0.05$) (Fig. 2, C and D). In addition, Arctic warming is amplified relative to global mean warming. Arctic precipitation changes, driven by thermodynamic factors, are similarly linked to warming in both historical and future periods (*2*, *3*). As Arctic warming intensifies, it triggers greater sea ice retreat, which in turn increases evaporation from the Arctic Ocean (*41*). According to the Clausius-Clapeyron equation, rising temperatures increase atmospheric water-holding capacity, promoting Arctic wetting. Figure 2 (E and F) highlights the strong correlation between global warming and Arctic wetting in

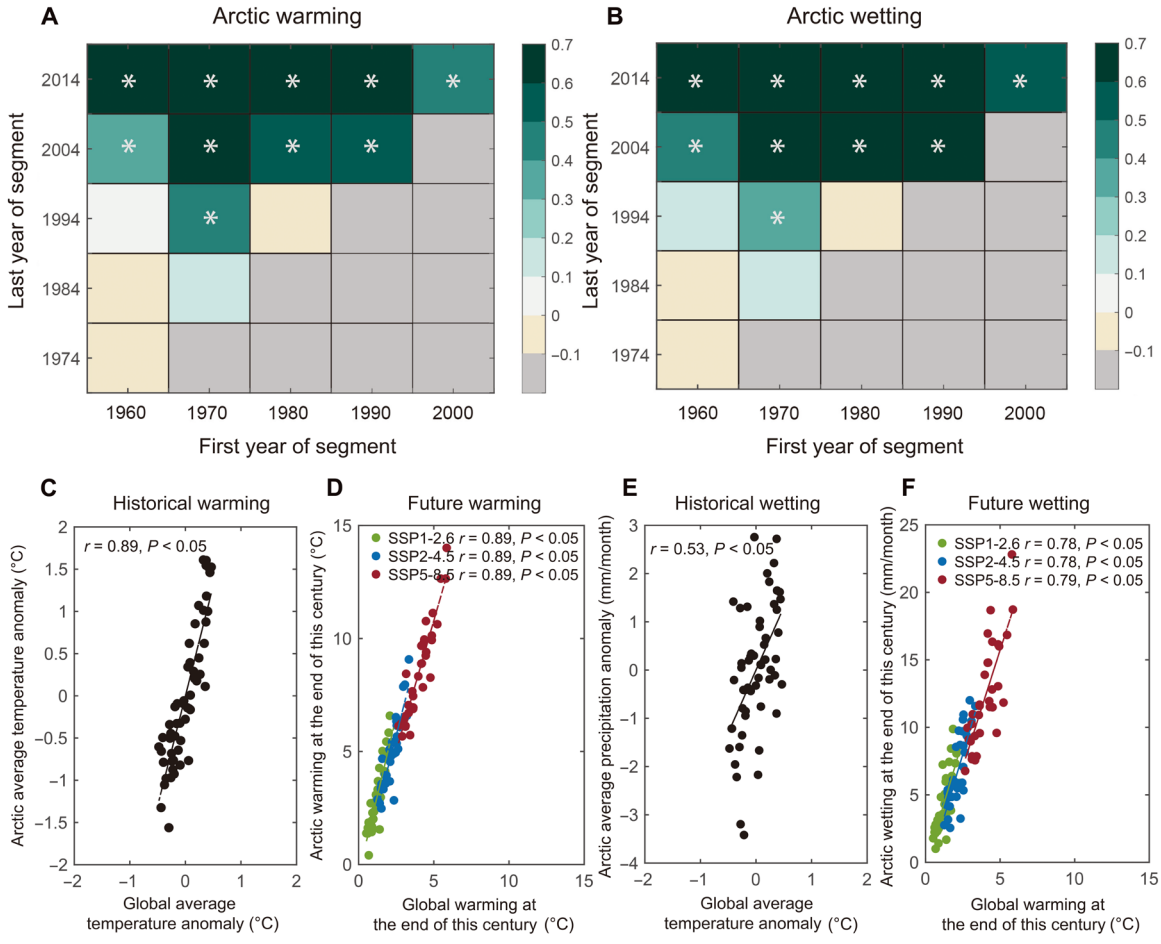

Fig. 2. The relationship between global warming trends and AWW. (**A** and **B**) Cross-models correlation coefficients between projections of Arctic average warming and wetting under the SSP5-8.5 scenario and simulated historical global warming trend, as a function of the start and ending year of historical trend calculation. The white asterisks indicate correlations that are significant at the 0.05 significance level. Gray cells represent missing data. (**C**) Scatter plot of observed global average temperature anomalies versus Arctic average temperature anomalies from 1960 to 2014. Each dot represents the annual anomaly relative to the mean value over the entire period. (**D**) Scatter plot of projected global warming versus Arctic average warming at the end of this century relative to the period 1995–2014 under the SSP1-2.6 (green), SSP2-4.5 (blue), and SSP5-8.5 (red) scenarios. Each dot represents a model. (**E**) and (**F**) are the same as (C) and (D) but for Arctic wetting. The historical temperature and precipitation results in (C) and (E) are derived from the ERA5 reanalysis data.

both historical periods ($r = 0.53$, $P < 0.05$) and future projections ($r = 0.78/0.78/0.79$ under SSP1-2.6/SSP2-4.5/SSP5-8.5, $P < 0.05$).

Given the close correlation between historical and future AWW with global warming, observed global warming can be used to constrain future AWW projections. As shown in Fig. 3, we demonstrate a relationship between historical global warming trends (1960 to 2014) and AWW at the end of this century. This indicates that future AWW projections in CMIP6 models are closely tied to the models' historical (and, by extension, future) global warming, a relationship that holds across all three scenarios.

To account for the influence of internal variability, we also examined results using only 11 single-model initial-condition large ensembles (SMILEs, represented by bold-edged dots in Fig. 3), each with more than 10 ensemble members. The ensemble means from these larger ensembles are less affected by internal variability than smaller ensembles and single realizations. The SMILEs support a substantial positive correlation between historical global warming and future AWW (gray line in Fig. 3), suggesting that AWW responses are associated with forced global warming and not solely due to internal variability, and further justifying this relationship as a reliable emergent constraint on future AWW.

We estimated the constrained magnitude of AWW using emergent constraint regression equations for each scenario. Probability density functions (PDFs; see Materials and Methods), fitted to Gaussian distributions, were drawn for both the original and constrained future AWW (fig. S2). The main constrained results are

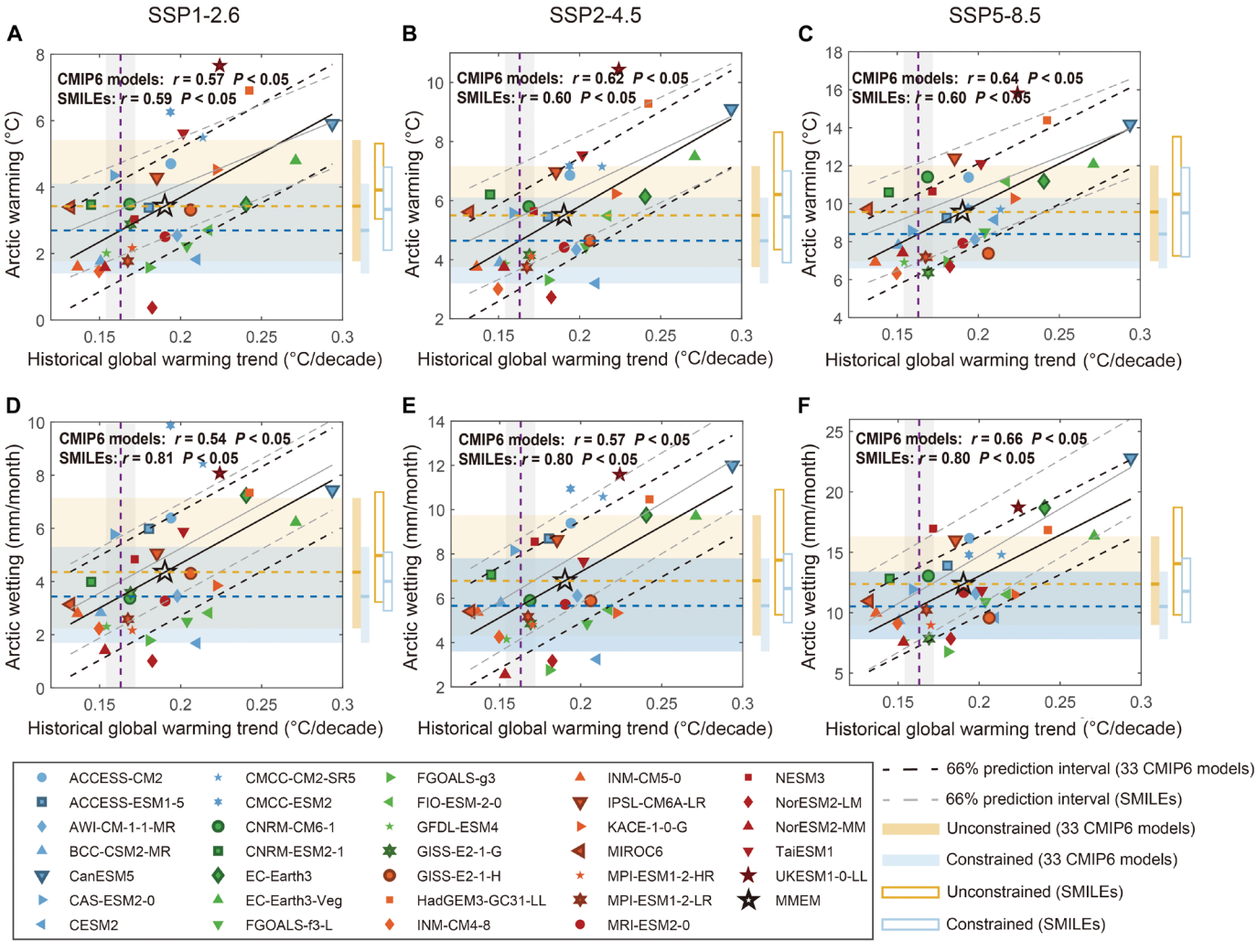

Fig. 3. Emergent constraints on the projected AWW based on the historical global warming trend. Scatter plot of Arctic (**A** to **C**) near-surface temperature and (**D** to **F**) total precipitation changes at the end of this century (relative to the period 1995–2014) under the SSP1-2.6, SSP2-4.5, and SSP5-8.5 scenarios among models versus historical global warming trend (1960 to 2014). The purple line shows observed (obtained from multiple observational datasets including ERA5, HadCRUT5, GISTEMP4, and BEST) global warming trend, with ±1σ uncertainty range (gray rectangle). The black pentagram represents the CMIP6 multi-model ensemble mean. The unconstrained/constrained mean projections are shown by the yellow/blue dashed line, and the yellow/blue rectangle indicates the likely range (17 to 83% likely range) of the future AWW before and after the emergent constraint, corresponding to the solid lines and shaded areas of the bar charts on the right side of each panel. The filled bars represent results using all models, while the unfilled bars represent results using only 11 SMILEs, represented by bold-edged dots). The black solid line represents the linear regression line, and the black dashed line represents the 66% confidence prediction interval. The gray solid/dashed lines represent the linear regression line, and its 66% confidence prediction interval is obtained using only 11 SMILEs.

based on the average of multiple observational datasets, although results from different observed estimates are also shown. All PDF curves indicate that the mean values of the constrained results are consistently lower across all scenarios, suggesting that the original projections overestimate future AWW. The constrained mean values, based on global warming from multiple datasets, are depicted as blue-shaded regions in Fig. 3. Compared to the original CMIP6 projections, the constrained mean outcomes decrease across all three emission scenarios. SMILEs show similar reductions in AWW. Under the SSP1-2.6, SSP2-4.5, and SSP5-8.5 scenarios, future Arctic average warming by the end of the 21st century decreases by 0.7°, 0.8°, and 1.1°C, respectively, compared to the original MMEM results. Meanwhile, future Arctic average wetting decreases by 0.9, 1.1, and 1.8 mm/month under the three scenarios.

In addition, the PDF curves in fig. S2 are narrower after applying the emergent constraint, which is due to the smaller observational uncertainty in historical global warming and the strong correlation between historical global warming and future AWW (*24*). For example, the uncertainty range for projected Arctic warming/wetting (blue shading compared to yellow in Fig. 3) decreases by 25/16%, 20/16%, and 26/23% under SSP1-2.6, SSP2-4.5, and SSP5-8.5, respectively. Constrained results using different observational datasets are detailed in table S2.

The overestimation of future AWW by the original models is linked to their overestimation of historical global warming. Compared to observational datasets (0.16° to 0.17°C per decade), the MMEM (0.19°C per decade) noticeably overestimated past global warming (fig. S3). However, since observations represent only one realization, the MMEM overestimation may not be entirely due to model errors. We analyzed all ensembles from each model, finding that nearly half of the models had all their ensembles above the observational range, including two SMILEs (CanESM5 and UKESM1-0-LL) (fig. S4). This finding aligns with studies showing that many CMIP6 models have high ECS values (*33*, *43*). By using observed historical global warming to constrain future AWW projections, we can correct the biases introduced by these models.

The linkage between historical sea ice pattern and future AWW local sensitivity pattern

The Arctic mean does not capture the geographical inhomogeneities in AWW. In the following section, we explore the concept of emergent constraints on the spatial patterns of AWW. To compare local changes across models with varying levels of AWW, we scale the spatial patterns of AWW by the average AWW, which we define as the "local sensitivity" (see Materials and Methods). It is evident that the inter-model spread in local sensitivity is concentrated in regions such as the Greenland Sea to the Barents-Kara seas (figs. S5 and S6). These areas experience the most intense interactions between sea ice, the atmosphere, and the ocean, with various feedback processes related to sea ice, open water, and ocean heat transport affecting the local sensitivity of AWW (*44*). Therefore, defining an emergent constraint taking these spatial inhomogeneities into account could improve the accuracy of spatial AWW projections.

Although strong correlations were found between historical global warming trends and local sensitivity in the central Arctic Ocean, this relationship was weak in other regions (fig. S7). This suggests that the historical global warming trend is not an effective constraint on local sensitivities (i.e., the spatial pattern of AWW). However, local sensitivities correlate well with historical SIC during the period 1979–2014. Notable correlations are found in the marginal seas near the historical ice edge, which coincide with areas of large inter-model spread of AWW. In particular, regions from the Greenland Sea to the Barents-Kara seas and from the East Siberian–Laptev seas to the Chukchi Sea show that models with higher historical SIC exhibit stronger future AWW. Conversely, in the central Arctic Ocean, especially near northern Greenland and the Canadian Archipelago, models with higher historical SIC show weaker future AWW (Fig. 4). This relationship can be explained by considering the current state of sea ice and its connection to future sea ice loss. Compared to observations, the MMEM of CMIP6 models overestimates SIC in the Greenland–Barents-Kara seas, and the simulated sea ice edge is positioned too far south (Fig. 5, A to C). The thickness of sea ice in the eastern Arctic is similarly overestimated (*45*). In these regions, global warming leads to greater sea ice loss because more ice is present to be lost—or, in some cases, ice is simulated where it does not exist. By the end of the century, sea ice in the marginal seas of the Arctic is expected to nearly disappear (*26*), meaning that the amount of sea ice loss will heavily depend on the amount of sea ice models simulated in the historical period. Conversely, in the central Arctic Ocean, models tend to slightly underestimate historical SIC, and those with less past sea ice project greater future sea ice loss (Fig. 5, D to F). In the northern regions of Greenland and the Canadian Archipelago, where sea ice is projected to persist at the century's end, future sea ice loss depends more on how models simulate sea ice sensitivity to warming, leading to correlations with historical global warming in this area. Studies have also shown that sea ice thickness in this region is similarly underestimated (*45*, *46*), implying higher sensitivity to warming and affecting future sea ice loss projections.

The reduction in sea ice enhances AWW through increased upward turbulent heat fluxes and evaporation over newly open water areas (*47*), as well as through atmospheric circulation anomalies driven by dynamic and thermodynamic processes (*39*, *48*, *49*), which shape the spatial pattern of AWW. To refine these projections, we developed a second emergent constraint based on the relationship between simulated historical SIC and local sensitivity. The results show that, in the Greenland–Barents-Kara seas—where inter-model spreads of warming and wetting local sensitivity are greatest—the adjusted local sensitivities are reduced compared to the original projections (fig. S8). This suggests that with the future disappearance of sea ice, models are projecting unrealistically high AWW in areas that, in reality, have little or no current ice cover. However, the situation is reversed near the Chukchi Sea, where historical SIC is underestimated. In the northern Canadian Archipelago, lower simulated SIC implies higher sensitivity to warming, leading to more future sea ice loss and exacerbating AWW. Consequently, adjusted warming and wetting local sensitivities in these regions have also been reduced (fig. S8).

Constraints on future AWW

Figures 6 and 7 show constrained projections for AWW, respectively, based on two constraints. The first constraint uses only historical global warming, while the second constraint incorporates the effect of historical SIC distribution on the local sensitivity in addition to the first constraint. The combination of these constraints, derived from historical global warming (obtained from multiple observational datasets) and the SIC spatial pattern, has reduced our estimates of Arctic average warming by the end of this century (fig. S9): The original projections of 3.4°C (1.8° to 5.4°C), 5.5°C (3.8° to 7.4°C), and 9.6°C (7.0° to 12.0°C) have been adjusted to 2.7°C (1.4° to

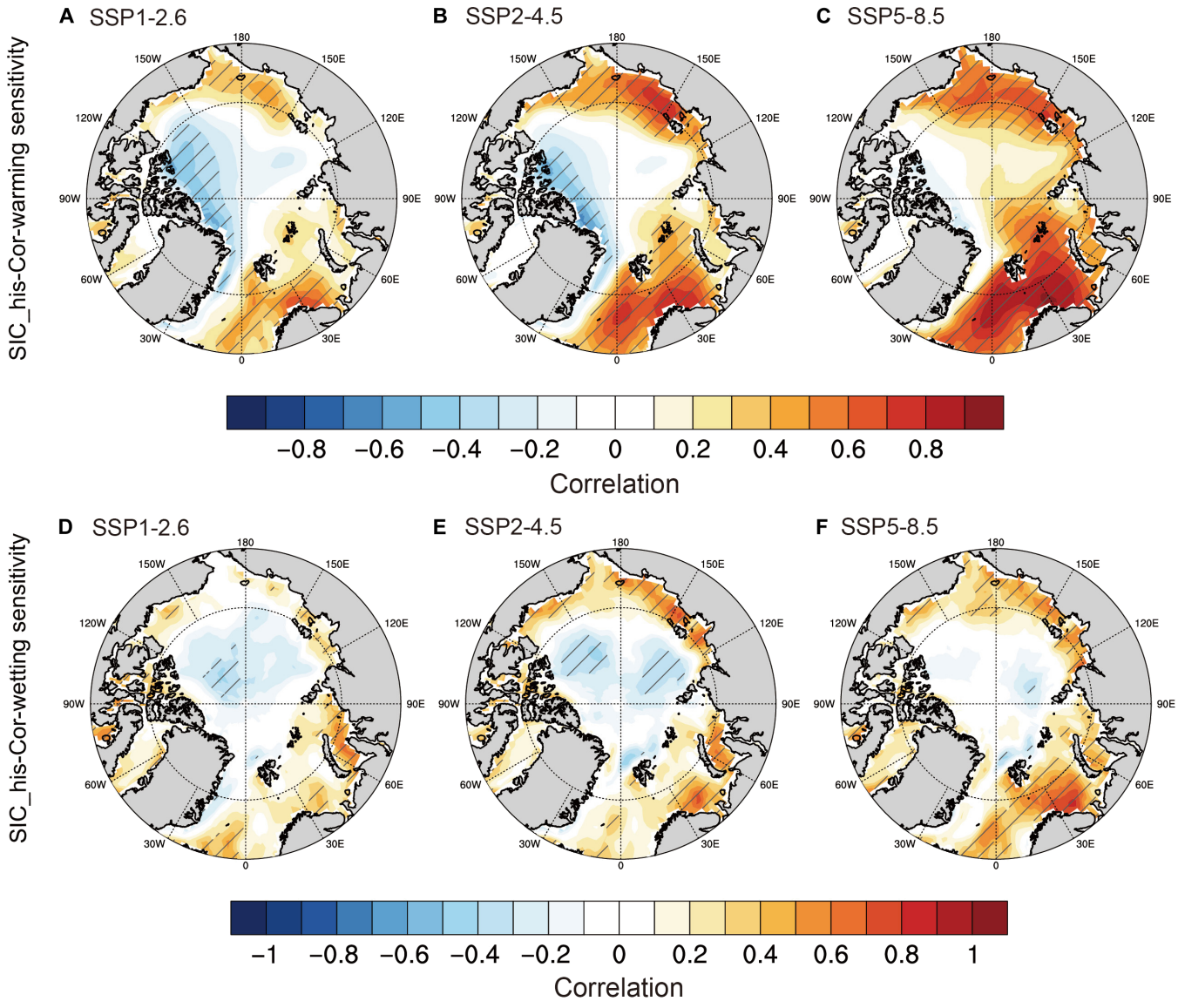

Fig. 4. The spatial relationship between historical Arctic SIC pattern and future local sensitivity pattern of AWW. (**A** to **C**) The correlations between the historical SIC pattern and the future Arctic warming local sensitivity pattern across models under the SSP1-2.6, SSP2-4.5, and SSP5-8.5 scenarios. (**D** to **F**) The same as (A) to (C) but for the Arctic wetting local sensitivity. The correlation is calculated at each grid point across models. The shading indicates the 95% confidence level of statistical significance. Local sensitivity is calculated as the warming and wetting at each grid point divided by the Arctic average.

4.0°C), 4.6°C (3.3° to 6.0°C), and 8.4°C (6.7° to 10.0°C) under the SSP1-2.6, SSP2-4.5, and SSP5-8.5 scenarios, respectively. Similarly, Arctic average wetting decreased from the unconstrained values of 4.4 (2.2 to 6.5) mm/month, 6.8 (4.3 to 9.3) mm/month, and 12.4 (8.8 to 16.0) mm/month to constrained values of 3.4 (1.6 to 5.4) mm/month, 5.7 (3.5 to 7.8) mm/month, and 10.5 (7.6 to 13.4) mm/month under the same scenarios. The results vary slightly across different observational datasets, but the overall reduction in AWW is consistent (table S3).

Regionally, over the Barents-Kara seas, the warming and wetting were reduced by 1.2°C and 1.7 mm/month, respectively, under the SSP2-4.5 scenario (Fig. 8 and table S4). In addition, uncertainties in the estimates for this region decreased by 35% for warming and 30% for wetting. Notable corrections were also observed in other regions: the East Siberian–Laptev seas (a decrease of 1.0°C and 1.0 mm/month), the Chukchi Sea (a decrease of 1.0°C and 1.2 mm/month), the Beaufort Sea (a decrease of 1.1°C and 1.1 mm/month), and the central Arctic Ocean (a decrease of 1.3°C and 1.6 mm/month). In these regions, the emergent constraint method substantially reduced the upper limits of future warming and wetting uncertainties. Similar results were observed for other emission scenarios (Fig. 8 and table S4). These findings demonstrate that the emergent constraint method, which combines historical global warming with the spatial pattern of SIC, is highly effective in constraining future AWW projections over the Arctic Ocean.

Figure 9 further highlights the impact of applying the second spatial constraint on top of the Arctic-mean constraint. While the

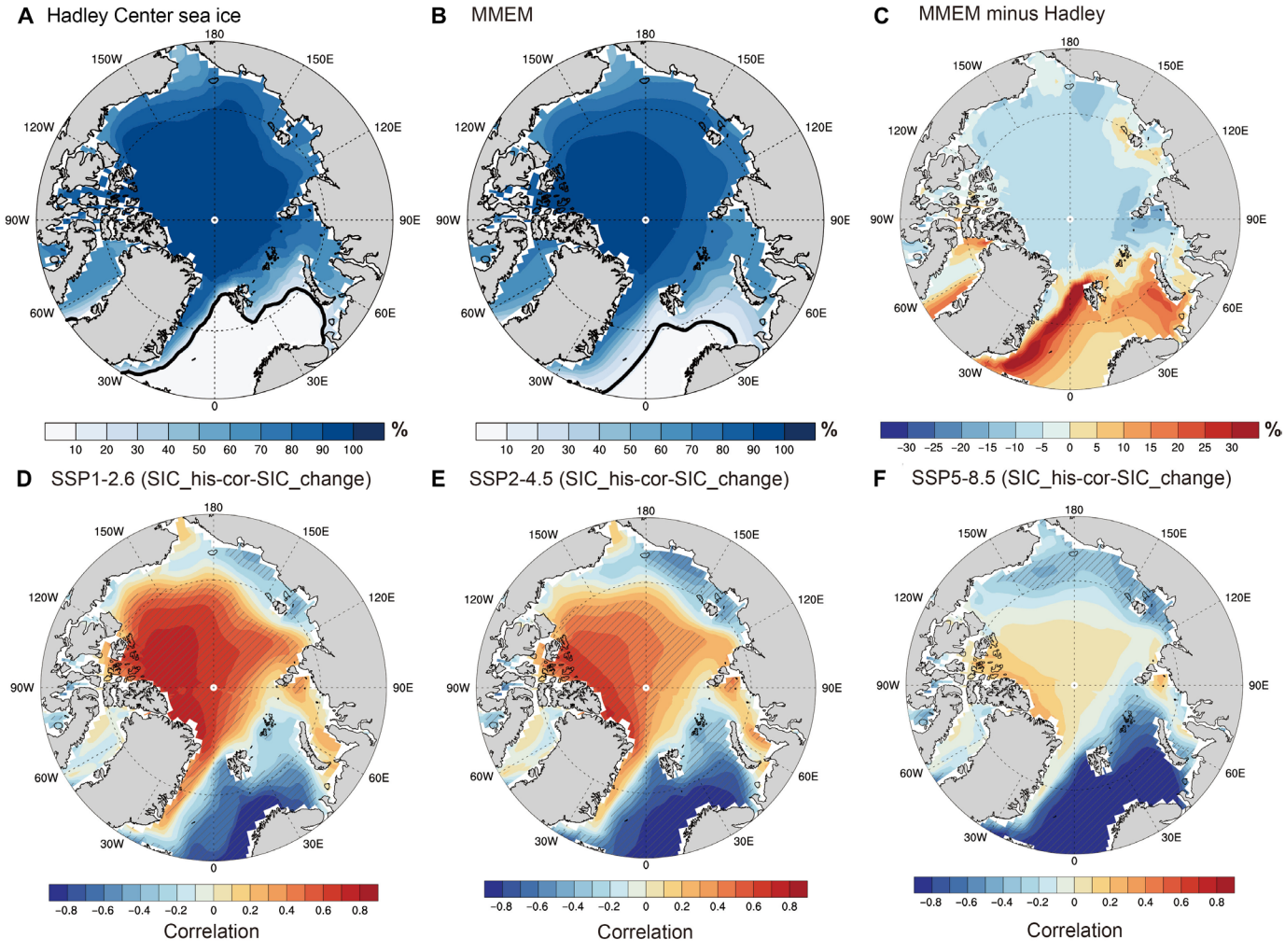

Fig. 5. The biases of simulated historical Arctic SIC pattern and the relationship between historical Arctic SIC and future sea ice loss. (**A**) Observed (Hadley) and (**B**) model-simulated average SIC from the MMEM of CMIP6 models and (**C**) its differences (MMEM minus Hadley) averaged over the period from 1979 to 2014. The black line represents the sea ice extent. (**D** to **F**) Spatial correlation between historical SIC and future sea ice change (SIC at the end of this century minus SIC during the historical period) across models under the SSP1-2.6, SSP2-4.5, and SSP5-8.5 scenarios. The correlation is calculated at each grid point across models.

second constraint, which accounts for SIC effects on local sensitivity, shows little difference in Arctic-mean warming and wetting compared to the first constraint, substantial differences are evident in specific sensitive regions, often offsetting each other. For example, the overestimation of future sea ice loss due to biases in historical SIC simulations leads to further downward adjustments in AWW projections in the Greenland–Barents-Kara seas by approximately 0.3°C/0.1 mm/month and 0.5°C/0.3 mm/month under the SSP2-4.5 and SSP5-8.5 scenarios, respectively. Conversely, underestimations of past SIC in the Chukchi Sea to the East Siberian Sea result in underestimations of future sea ice loss in these areas, prompting upward adjustments of AWW projections compared to the first constraint. In addition, underestimations of historical SIC in the northern Canadian Archipelago lead to slight downward adjustments in warming and wetting under moderate to low emission scenarios (Fig. 9). These results underscore the importance of applying the second spatial constraint to more accurately constrain the spatial patterns of AWW.

DISCUSSION

In summary, this study developed emergent constraints on projected AWW by examining the relationships between historical global warming trends, mean sea ice state, and future AWW across 33 CMIP6 models under the SSP1-2.6, SSP2-4.5, and SSP5-8.5 scenarios. The constrained results reveal that the original CMIP6 models overestimate future AWW, particularly in the Barents-Kara seas under high-emission scenarios, due to their higher global warming trends and excessive historical SIC. In addition, the uncertainty ranges for Arctic warming and Arctic wetting are narrowed by about 25 to 4% and 12 to 19%. Uncertainties in warming and wetting are reduced by approximately one-third in the Barents-Kara seas, East Siberian–Laptev seas, Chukchi Sea, Beaufort Sea, and the central Arctic Ocean—about three times greater than the uncertainty reduction over the Arctic land areas. These findings also suggest that the faster AWW seen in previous comparisons between CMIP6 and CMIP5 models may be attributed to model

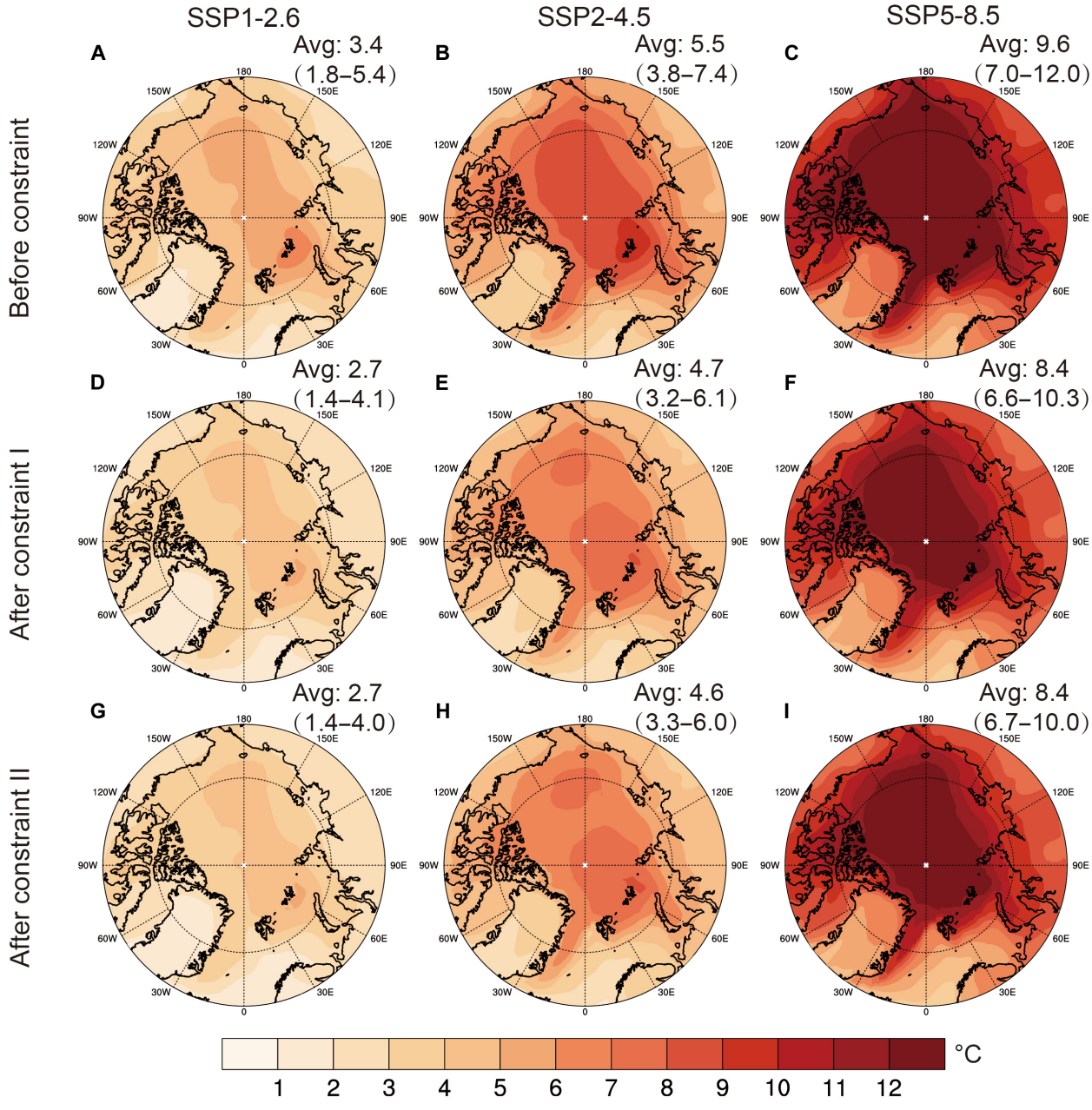

Fig. 6. Emergent constraints on the projected Arctic warming pattern at the end of this century. The spatial pattern of Arctic warming at the end of this century (**A** to **C**) before applying constraints, (**D** to **F**) after constraint I, and (**G** to **I**) after constraint II under the SSP1-2.6, SSP2-4.5, and SSP5-8.5 scenarios are shown. The numbers in the upper right corners represent the Arctic average results from the MMEM, and the numbers in parentheses represent the 17 to 83% likely range. "After constraint I" represents the constraint result based on global warming trend, while "After constraint II" represents the combined constraint results based on global warming trend and SIC distribution.

biases, as our constrained results align more closely with CMIP5 projections (*4*).

We considered that uncertainties in simulated global warming trends could affect AWW projections. The emergent constraint relationship assumes that the associated physical processes change linearly with climate change and are well represented in the models. We use the past global warming trend as a constraint factor for future AWW, driven by increased CO_2 concentrations, based on the fact that, to a first approximation, the global temperature response is proportional to radiative forcing. Stronger climate feedbacks mean both past and future warming intensify as forcing increases (*50*). Although the relationship between past and future warming might be obscured by compensatory climate feedbacks and uncertainties in aerosol forcing (*33*), recent decades of global warming and projected warming by the end of this century have been shown to be primarily driven by greenhouse gases (*42*, *51*). As a product of global warming, the long-term changes of AWW in both the past and the future are also considered to be primarily influenced by greenhouse

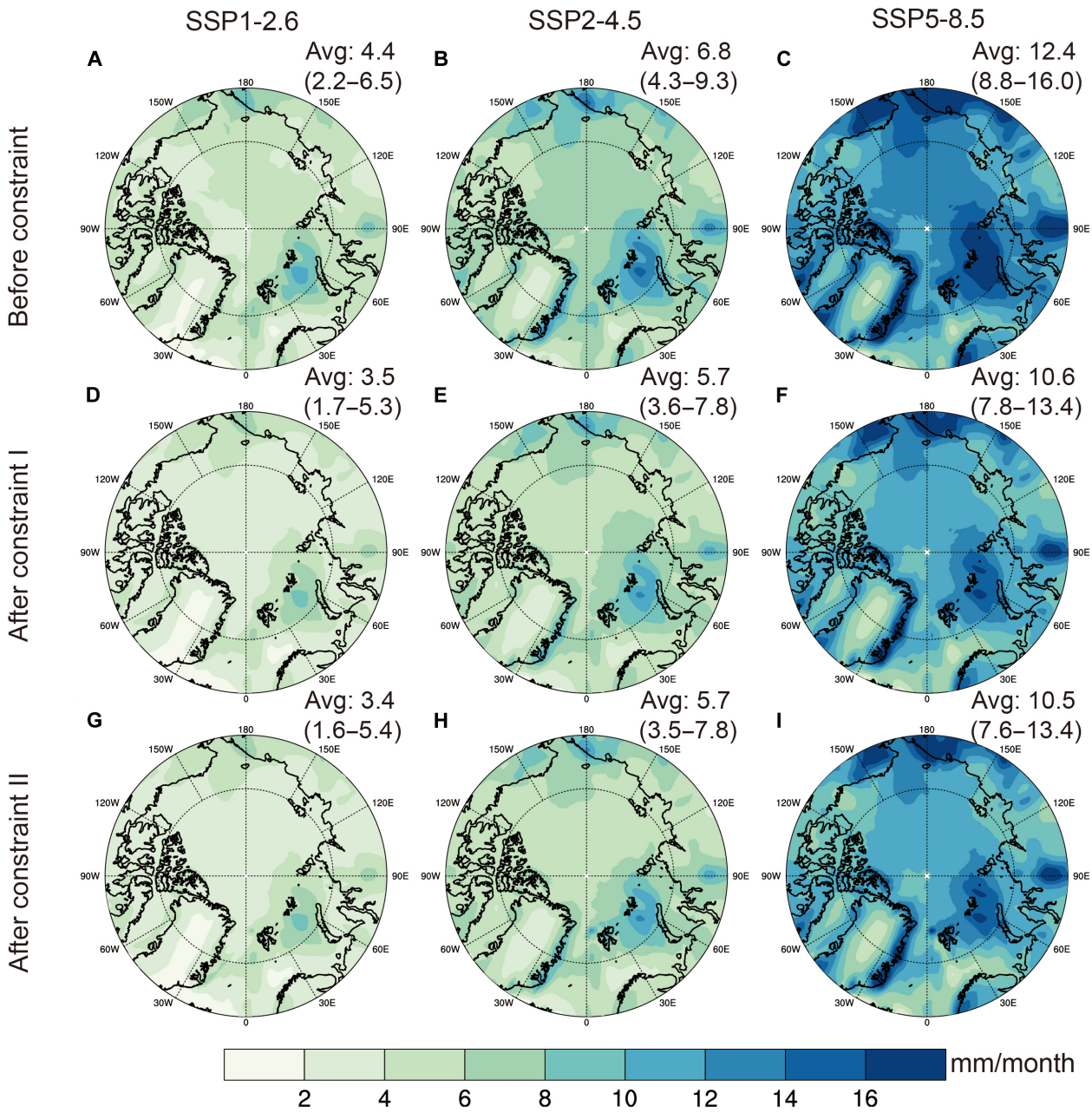

Fig. 7. Emergent constraints on the projected Arctic wetting pattern at the end of this century. The spatial pattern of Arctic wetting at the end of this century (**A** to **C**) before applying constraints, (**D** to **F**) after constraint I, and (**G** to **I**) after constraint II under the SSP1-2.6, SSP2-4.5, and SSP5-8.5 scenarios. The numbers in the upper right corners represent the Arctic average results from the MMEM, and the numbers in parentheses represent the 17 to 83% likely range. "After constraint I" represents the constraint result based on global warming trend, while "After constraint II" represents the combined constraint results based on global warming trend and SIC distribution.

gases (*14*, *52*, *53*). Thus, the notable positive correlation between global warming and AWW is evident in both the past and the future (Fig. 2). Many studies have also shown that CMIP6 models tend to exhibit high ECS, with models featuring high ECS showing stronger recent and future warming both globally and in the Arctic (*29*, *33*, *43*, *54*). Moreover, even against the backdrop of rapid Arctic climate change, the Arctic radiative response may remain stable (*55*). These indicate that the feedback between higher global warming and stronger AWW will persist in the future, and the Arctic climate responses to external forcing may be similar to the current climate, ensuring that the emergent constraint relationship remains valid. Considering the overestimation of sea ice in the marginal Arctic Ocean under current climate conditions, there is a risk of overestimating sea ice loss in these regions by the end of this century, which could lead to unrealistic projections of warming and wetting. To address this, we made further adjustments to the local sensitivity of future AWW when considering the spatial pattern.

However, we cannot ignore biases in the sensitivity of sea ice to warming (*56*) and uncertainties in the contribution of sea ice loss to AWW in the models (*57*–*59*). For instance, one study indicated that

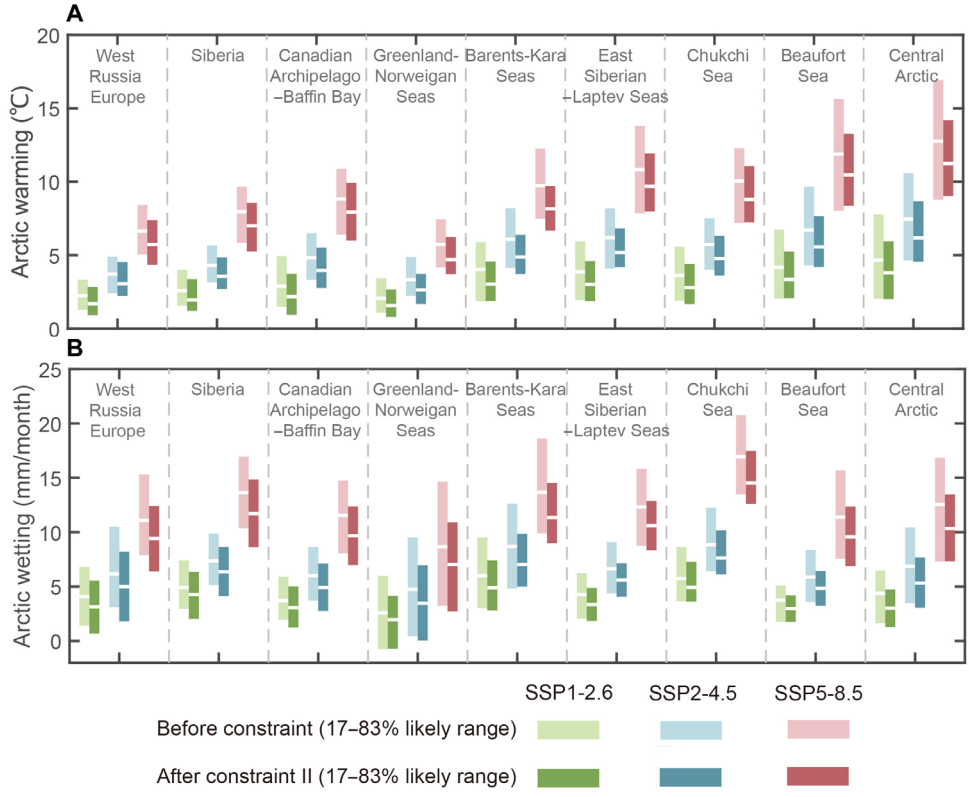

Fig. 8. Emergent constraints on the projected AWW in each region of the Arctic at the end of this century. (**A**) Regionally averaged warming in Arctic subregions before (light color) and after constraint II (dark color). (**B**) Regionally averaged wetting in Arctic subregions before (light color) and after constraint II (dark color). The horizontal line represents the MMEM result, and the shaded area represents the 17 to 83% likely range.

CMIP6 models underestimate the impact of SIC on sensible heat fluxes, which could influence projections of Arctic warming, especially during winter (*60*). Therefore, we also explored whether historical Arctic amplification, largely driven by sea ice albedo feedback, has an emergent constraint relationship with future AWW but found no notable correlation (fig. S10). This may be due to the fact that some models predict ice-free conditions by the end of the century (*26*), causing the primary drivers of Arctic amplification to shift—Nonlocal factors such as ocean heat transport may become more dominant (*61*). While historical sea ice albedo feedback effectively constrains projections for the coming decades, this emergent constraint relationship weakens over time (*62*). As this study focuses on AWW at the end of the century, the global warming trends related to ECS and the distribution of historical sea ice are more effective emergent factors compared to uncertainties in simulated Arctic amplification.

In addition to using emergent constraints to reduce the uncertainty of future AWW projections, previous studies have applied methods such as model selection and reweighting based on historical simulation performance. These methods have similarly found an overestimation of future AWW (*2*, *22*). However, because of differences in baseline data and definitions of future periods, directly comparing the effectiveness of these methods in constraining future AWW is challenging. That said, when compared to the results of a previous study (*2*) using the same data, the magnitudes of Arctic wetting adjustments obtained through the emergent constraint technique are greater than those from model reweighting methods. Furthermore, while the previous constrained results also indicated an overestimation of Arctic warming projections (*29*), our study uniquely applies the emergent constraint method to Arctic wetting and considers the impact of local sea ice changes on spatial patterns, extending the constrained projections to Arctic subregions. The constrained spatial pattern of AWW emphasizes the uneven effectiveness of traditional constraints across different regions, which will be of great value for future climate projections, impact assessments, and adaptation strategies in specific Arctic regions.

MATERIALS AND METHODS

Data

Arctic near-surface temperature and precipitation data were derived from monthly 2-m temperature and total precipitation outputs from the ERA5 (*63*), with a horizontal resolution of about 0.25° × 0.25°, covering the period from 1960 onward. Observed sea ice data are obtained from the Hadley Centre, with a horizontal resolution of 1° × 1° (*64*). Arctic sea ice extent is defined as the total area of grid cells with an SIC greater than 15%. The observed global warming trend from 1960 to 2014 was calculated using four datasets: ERA5, Met Office Hadley Centre global surface temperature anomalies version 5 (HadCRUT5) (*65*), GISS surface temperature analysis version 4 (GISTEMP4) (*66*), and Berkeley Earth Surface Temperature (BEST) (*67*).

In addition, we collected monthly near-surface air temperature, total precipitation, and SIC outputs from the historical and Scenario Model Intercomparison Project experiments of 33 CMIP6 models

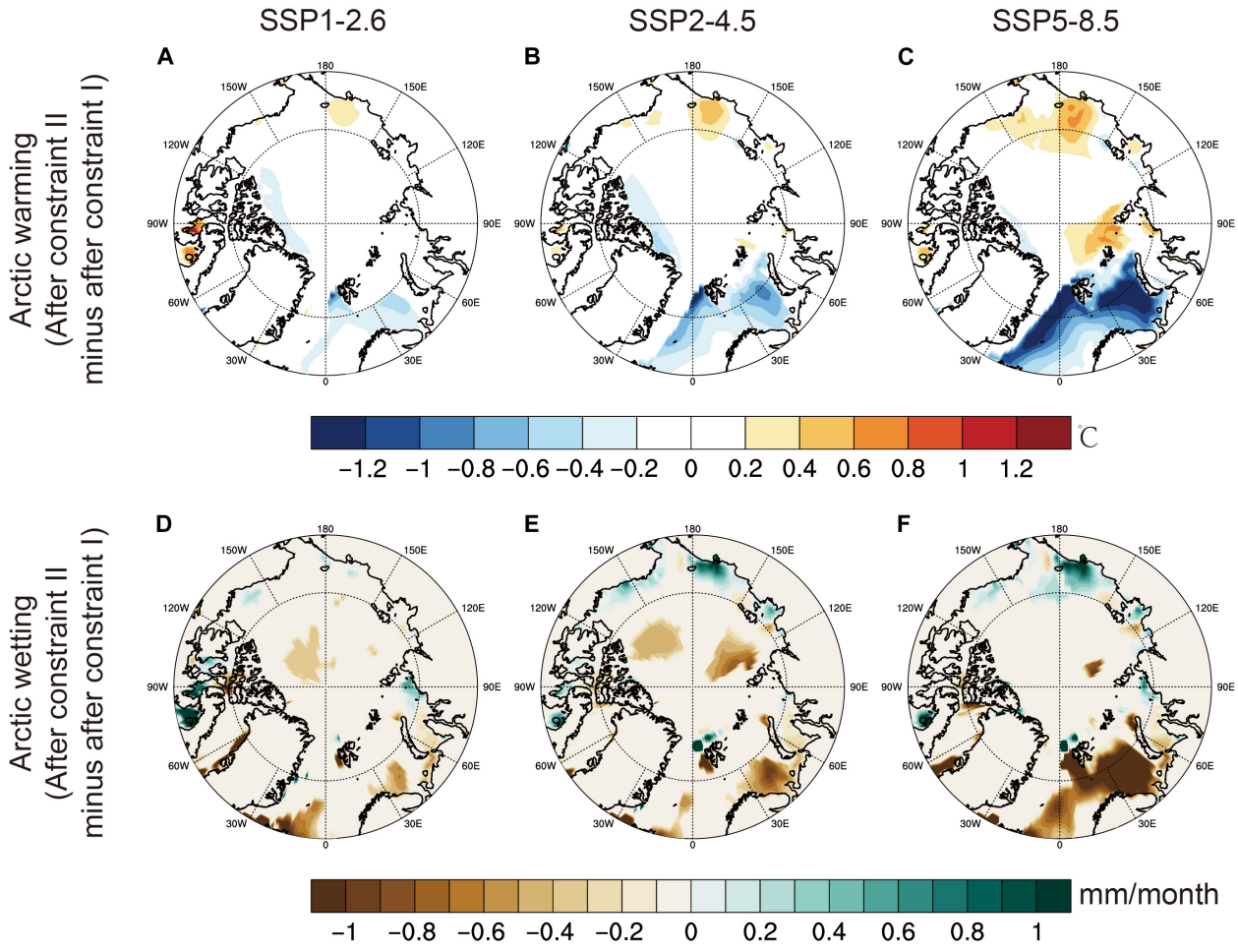

Fig. 9. Spatial patterns of emergent constraint effects based on historical SIC pattern on AWW. The differences in the spatial patterns of (**A** to **C**) Arctic warming and (**D** to **F**) Arctic wetting between applying constraints from both historical global warming and SIC (After constraint II) compared to using only historical global warming constraints (After constraint I).

(table S1). Models were selected on the basis of the availability of required variables and scenarios (both historical and future SSP1-2.6, SSP2-4.5, and SSP5-8.5 scenarios) and are consistent with those used in our previous projection study (*2*) for comparison of results. Note that SIC data were not available for AWI-CM1-1-MR and KACE-1-0-G, so sea ice data were provided by only 31 models. The simulations span from 1960 to 2014 for historical experiments and 2015 to 2100 for future projections based on three shared SSPs: SSP1-2.6, SSP2-4.5, and SSP5-8.5 (*68*).

Given the varying spatial resolutions among CMIP6 models, we regridded each model's outputs to a uniform horizontal resolution of 1° × 1°. We calculated the ensemble mean for each model to avoid bias toward models with more simulations and to reduce internal variability. However, eight models have only one ensemble member, and others have fewer than five members, meaning that internal variability may be higher in these models.

Definition of future AWW and local sensitivity to AWW

The Arctic region is defined in this study as the area north of 66°N. The subregions of the Arctic Ocean were determined following McCrystal *et al.* (*4*), divided into nine regions: West Russia and Europe, Siberia, Canadian Archipelago–Baffin Bay, Greenland-Norweigan seas, Barents-Kara seas, East Siberian–Laptev seas, Chukchi Sea, Beaufort Sea, and Central Arctic (fig. S1).

We calculated the regional average annual changes in Arctic warming $(\Delta\overline{T})$ and wetting $(\Delta\overline{P})$ at the end of this century (2081–2100) relative to the historical period (1995–2014, the reference period for IPCC AR6), defined as the future AWW changes. Furthermore, to reflect the spatial pattern information, we calculated the local sensitivity of warming $\left[sT_{(i,j)}\right]$ and wetting $\left[sP_{(i,j)}\right]$ for each grid point by scaling the average AWW

$$sT_{(i,j)} = \frac{\Delta T_{(i,j)}}{\Delta\overline{T}} \quad (1)$$

$$sP_{(i,j)} = \frac{\Delta P_{(i,j)}}{\Delta\overline{P}} \quad (2)$$

Observational constraints on future projections

The emergent constraint method relies on linear relationships between observable historical simulation variables (x) and future climate projection variables (y) across ensembles of models (*25*). Since observational data generally have less uncertainty compared to

model simulations, it provides more reliable insights into temporal and spatial changes. By projecting the observed value of x_0 (with its associated uncertainty, typically represented by one SD) onto y through the established linear relationship and incorporating the prediction error of the regression model, we can achieve more accurate projections of y with reduced uncertainty (*35*). In this study, y represents AWW by the end of this century, while x denotes the global warming trend from 1960 to 2014 and the SIC mean state from 1979 to 2014. The emergent constraint relationship is derived using least-squares linear regression across models

$$f(x_n) = ax_n + b \tag{3}$$

where a and b are the slope and intercept values, respectively, and the linear regression $f(x_n)$ given by y_n and x_n is defined by a and b. The n index represents different models. The prediction error of the regression (σ_y) is calculated as follows (*25*)

$$\sigma_y(x) = \sqrt{s^2\left[1 + \frac{1}{N} + \frac{(x_n - \bar{x})^2}{N \times \sigma_x^2}\right]} \tag{4}$$

where N is the number of models, the n index represents different models, and $\bar{x}$ represents the mean value of models. The least-squares error (s^2) and the SD of x_n (σ_x) are calculated as follows

$$s^2 = \frac{1}{N-2}\sum_{n=1}^{N}\left[y_n - f(x_n)\right]^2 \tag{5}$$

$$\sigma_x = \sqrt{\sum_{n=1}^{N}(x_n - \bar{x})^2 / N} \tag{6}$$

Therefore, Eq. 3 can be used to adjust the original projections of y to y_0 using the observed variable x_0

$$y_0 = ax_0 + b \tag{7}$$

When substituting $x = x_0$ in Eq. 4, the x-adjusted regression prediction error can be obtained.

In addition, according to the previously established method (*25*, *27*), for a linear regression based on the assumption that the error of the regression is normally distributed the Gaussian PDF around the best-fit linear regression can be calculated as follows, which represents the PDF of y given x

$$PDF(y \mid x) = \frac{1}{\sqrt{2\pi\sigma_y^2}} exp\left\{-\frac{\left[y - f(x)\right]^2}{2\sigma_y^2}\right\} \tag{8}$$

Then, the PDF for the constrained projected variable [$PDF(Y)$] is calculated by numerically integrating $PDF(y/x_0)$ and $PDF(x_0)$

$$PDF(Y) = \int_{-\infty}^{+\infty} PDF(y/x_0)\,PDF(x_0)\,dx_0 \tag{9}$$

where $PDF(y/x_0)$ is the probability density for the "future projected variable" given the "historical observed variable", and $PDF(x_0)$ is the observation-based PDF for the historical observed variable.

The future spatial pattern of AWW is influenced by both the Arctic average change and the local sensitivity (see the local sensitivity calculation method above). This study presents the spatial patterns after applying two emergent constraints. The first constraint uses only historical global warming to constrain the Arctic average change, with local sensitivities remaining unchanged, resulting in a consistent emergent constraint relationship across horizontal space. More specifically, the change at each grid point is treated as the product of the Arctic average change and local sensitivity (as calculated above for local sensitivity), and the constraint relationship between historical global warming and Arctic average change remains consistent for each grid point. The second constraint incorporates the effect of past SIC distribution on future AWW local sensitivity, building on the first Arctic mean constraint. In this case, x_n and y_n in Eq. 3 become functions of horizontal space, creating an emergent constraint relationship that varies across space.

Furthermore, by selecting the 83 and 17% thresholds from the cumulative probability density distribution, the range between these thresholds defines the projected likely range, and the difference between them defines the uncertainty range. The difference between the mean values before and after applying the constraint represents the correction due to the emergent constraint. The reduction in uncertainty is calculated as

$$\text{Reduced uncertainty in AWW} = \frac{(\text{Unconstrained uncertainty range of AWW} - \text{Constrained uncertainty range of AWW})}{\text{Unconstrainted uncertainty range of AWW}} \times 100\% \tag{10}$$

Supplementary Materials

This PDF file includes:

Figs. S1 to S10

Tables S1 to S4

REFERENCES AND NOTES

1. M. Rantanen, A. Y. Karpechko, A. Lipponen, K. Nordling, O. Hyvarinen, K. Ruosteenoja, T. Vihma, A. Laaksonen, The Arctic has warmed nearly four times faster than the globe since 1979. *Commun. Earth Environ.* **3**, 168 (2022).
2. Z. Cai, Q. You, H. W. Chen, R. Zhang, Z. Zuo, D. Chen, J. Cohen, J. A. Screen, Assessing Arctic wetting: Performances of CMIP6 models and projections of precipitation changes. *Atmos. Res.* **297**, 107124 (2024).
3. T. F. Dou, S. F. Pan, R. Bintanja, C. D. Xiao, More frequent, intense, and extensive rainfall events in a strongly warming arctic. *Earths Future* **10**, e2021EF002378 (2022).
4. M. R. McCrystall, J. Stroeve, M. Serreze, B. C. Forbes, J. A. Screen, New climate models reveal faster and larger increases in Arctic precipitation than previously projected. *Nat. Commun.* **12**, 6765 (2021).
5. Q. You, Z. Cai, N. Pepin, D. Chen, B. Ahrens, Z. Jiang, F. Wu, S. Kang, R. Zhang, T. Wu, P. Wang, M. Li, Z. Zuo, Y. Gao, P. Zhai, Y. Zhang, Warming amplification over the Arctic Pole and Third Pole: Trends, mechanisms and consequences. *Earth Sci. Rev.* **217**, 103625 (2021).
6. H. Park, E. Watanabe, Y. Kim, I. Polyakov, K. Oshima, X. Zhang, J. S. Kimball, D. Yang, Increasing riverine heat influx triggers Arctic sea ice decline and oceanic and atmospheric warming. *Sci. Adv.* **6**, eabc4699 (2020).
7. J. Mouginot, E. Rignot, A. A. Bjork, M. van den Broeke, R. Millan, M. Morlighem, B. Noël, B. Scheuchl, M. Wood, Forty-six years of Greenland Ice Sheet mass balance from 1972 to 2018. *Proc. Natl. Acad. Sci. U.S.A.* **116**, 9239–9244 (2019).
8. R. G. M. Spencer, P. J. Mann, T. Dittmar, T. I. Eglinton, C. McIntyre, R. M. Holmes, N. Zimov, A. Stubbins, Detecting the signature of permafrost thaw in Arctic rivers. *Geophys. Res. Lett.* **42**, 2830–2835 (2015).
9. X. Zhang, J. He, J. Zhang, I. Polyakov, R. Gerdes, J. Inoue, P. Wu, Enhanced poleward moisture transport and amplified northern high-latitude wetting trend. *Nat. Clim. Change* **3**, 47–51 (2013).
10. E. Post, R. B. Alley, T. R. Christensen, M. Macias-Fauria, B. C. Forbes, M. N. Gooseff, A. Iler, J. T. Kerby, K. L. Laidre, M. E. Mann, J. Olofsson, J. C. Stroeve, F. Ulmer, R. A. Virginia, M. Wang, The polar regions in a 2°C warmer world. *Sci. Adv.* **5**, eaaw9883 (2019).

11. J. Cohen, X. Zhang, J. Francis, T. Jung, R. Kwok, J. Overland, T. J. Ballinger, U. S. Bhatt, H. W. Chen, D. Coumou, S. Feldstein, H. Gu, D. Handorf, G. Henderson, M. Ionita, M. Kretschmer, F. Laliberte, S. Lee, H. W. Linderholm, W. Maslowski, Y. Peings, K. Pfeiffer, I. Rigor, T. Semmler, J. Stroeve, P. C. Taylor, S. Vavrus, T. Vihma, S. Wang, M. Wendisch, Y. Wu, J. Yoon, Divergent consensuses on Arctic amplification influence on midlatitude severe winter weather. *Nat. Clim. Change* **10**, 20–29 (2020).
12. D. Coumou, G. Di Capua, S. Vavrus, L. Wang, S. Wang, The influence of Arctic amplification on mid-latitude summer circulation. *Nat. Commun.* **9**, 2959 (2018).
13. J. A. Francis, S. J. Vavrus, Evidence linking Arctic amplification to extreme weather in mid-latitudes. *Geophys. Res. Lett.* **39**, L06801 (2012).
14. Z. Cai, Q. You, F. Wu, H. W. Chen, D. Chen, J. Cohen, Arctic warming revealed by multiple CMIP6 models: Evaluation of historical simulations and quantification of future projection uncertainties. *J. Climate* **34**, 4871–4892 (2021).
15. R. Davy, S. Outten, The Arctic surface climate in CMIP6: Status and developments since CMIP5. *J. Climate* **33**, 8047–8068 (2020).
16. D. Notz, SIMIP Community, Arctic sea ice in CMIP6. *Geophys. Res. Lett.* **47**, e2019GL086749 (2020).
17. M. Long, L. Zhang, S. Hu, S. Qian, Multi-aspect assessment of CMIP6 models for arctic sea ice simulation. *J. Climate* **34**, 1515–1529 (2021).
18. Z. Shen, A. Duan, D. Li, J. Li, Assessment and ranking of climate models in Arctic Sea Ice cover simulation: From CMIP5 to CMIP6. *J. Climate* **34**, 3609–3627 (2021).
19. X. Hu, H. Fan, M. Cai, S. A. Sejas, P. Taylor, S. Yang, A less cloudy picture of the inter-model spread in future global warming projections. *Nat. Commun.* **11**, 4472 (2020).
20. Q. Zhang, B. Huai, M. Ding, W. Sun, W. Liu, J. Yan, S. Zhao, Y. Wang, Y. Wang, L. Wang, J. Che, J. Dou, L. Kang, Projections of Greenland climate change from CMIP5 and CMIP6. *Glob. Planet. Change* **232**, 104340 (2024).
21. J. Räisänen, L. Ruokolainen, J. Ylhaisi, Weighting of model results for improving best estimates of climate change. *Climate Dynam.* **35**, 407–422 (2010).
22. T. J. Bracegirdle, D. B. Stephenson, Higher precision estimates of regional polar warming by ensemble regression of climate model projections. *Climate Dynam.* **39**, 2805–2821 (2012).
23. V. Eyring, P. M. Cox, G. M. Flato, P. J. Gleckler, G. Abramowitz, P. Caldwell, W. D. Collins, B. K. Gier, A. D. Hall, F. M. Hoffman, G. C. Hurtt, A. Jahn, C. D. Jones, S. A. Klein, J. P. Krasting, L. Kwiatkowski, R. Lorenz, E. Maloney, G. A. Meehl, A. G. Pendergrass, R. Pincus, A. C. Ruane, J. L. Russell, B. M. Sanderson, B. D. Santer, S. C. Sherwood, I. R. Simpson, R. J. Stouffer, M. S. Williamson, Taking climate model evaluation to the next level. *Nat. Clim. Change* **9**, 102–110 (2019).
24. A. Hall, P. Cox, C. Huntingford, S. Klein, Progressing emergent constraints on future climate change. *Nat. Clim. Change* **9**, 269–278 (2019).
25. P. M. Cox, C. Huntingford, M. S. Williamson, Emergent constraint on equilibrium climate sensitivity from global temperature variability. *Nature* **553**, 319–322 (2018).
26. A. Jahn, M. M. Holland, J. E. Kay, Projections of an ice-free Arctic Ocean. *Nat. Rev. Earth Environ.* **5**, 164–176 (2024).
27. Z. Shen, W. Zhou, J. Li, J. C. L. Chan, A frequent ice-free Arctic is likely to occur before the mid-21st century. *Npj Clim. Atmos. Sci.* **6**, 103 (2023).
28. D. Topál, Q. Ding, Atmospheric circulation-constrained model sensitivity recalibrates Arctic climate projections. *Nature climate change* **13**, 710–718 (2023).
29. X. M. Hu, J. R. Ma, J. Ying, M. Cai, Y. Q. Kong, Inferring future warming in the Arctic from the observed global warming trend and CMIP6 simulations. *Adv. Clim. Change Res.* **12**, 499–507 (2021).
30. O. Linke, N. Feldl, J. Quaas, Current-climate sea ice amount and seasonality as constraints for future Arctic amplification. *Environ. Res. Clim.* **2**, 045003 (2023).
31. Z. Hausfather, K. Marvel, G. A. Schmidt, J. W. Nielsen-Gammon, M. Zelinka, Climate simulations: Recognize the 'hot model' problem. *Nature* **605**, 26–29 (2022).
32. P. Voosen, 'Hot' climate models exaggerate Earth impacts. *Science* **376**, 685–685 (2022).
33. K. B. Tokarska, M. B. Stolpe, S. Sippel, E. M. Fischer, C. J. Smith, F. Lehner, R. Knutti, Past warming trend constrains future warming in CMIP6 models. *Sci. Adv.* **6**, eaaz9549 (2020).
34. H. Shiogama, M. Watanabe, H. Kim, N. Hirota, Emergent constraints on future precipitation changes. *Nature* **602**, 612–616 (2022).
35. Y. Chai, Y. Yue, L. J. Slater, J. Yin, A. G. L. Borthwick, T. Chen, G. Wang, Constrained CMIP6 projections indicate less warming and a slower increase in water availability across Asia. *Nat. Commun.* **13**, 4124 (2022).
36. Z. Chen, T. Zhou, X. Chen, W. Zhang, L. Zhang, M. Wu, L. Zou, Observationally constrained projection of Afro-Asian monsoon precipitation. *Nat. Commun.* **13**, 2552 (2022).
37. P. Dai, J. Nie, Y. Yu, R. Wu, Constraints on regional projections of mean and extreme precipitation under warming. *Proc. Natl. Acad. Sci. U.S.A.* **121**, e2312400121 (2024).
38. Q. Sun, C. Miao, Q. Duan, H. Ashouri, S. Sorooshian, K.-L. Hsu, A review of global precipitation data sets: Data sources, estimation, and intercomparisons. *Rev. Geophys.* **56**, 79–107 (2018).
39. R. C. Boeke, P. C. Taylor, Seasonal energy exchange in sea ice retreat regions contributes to differences in projected Arctic warming. *Nat. Commun.* **9**, 5017 (2018).
40. R. Bintanja, The impact of Arctic warming on increased rainfall. *Sci. Rep.* **8**, 16001 (2018).
41. R. Bintanja, F. M. Selten, Future increases in Arctic precipitation linked to local evaporation and sea-ice retreat. *Nature* **509**, 479–482 (2014).
42. IPCC, Summary for policymakers, in Climate Change 2021: The Physical Science Basis. Contribution of Working Group I to the Sixth Assessment Report of the Intergovernmental Panel on Climate Change. (2021).
43. M. D. Zelinka, T. A. Myers, D. T. McCoy, S. Po-Chedley, P. M. Caldwell, P. Ceppi, S. A. Klein, K. E. Taylor, Causes of higher climate sensitivity in CMIP6 models. *Geophys. Res. Lett.* **47**, e2019GL085782 (2020).
44. J. A. Screen, C. Deser, D. M. Smith, X. Zhang, R. Blackport, P. J. Kushner, T. Oudar, K. E. McCusker, L. Sun, Consistency and discrepancy in the atmospheric response to Arctic sea-ice loss across climate models. *Nat. Geosci.* **11**, 155–163 (2018).
45. L. Chen, R. Wu, Q. Shu, C. Min, Q. Yang, B. Han, The Arctic Sea Ice thickness change in CMIP6's historical simulations. *Adv. Atmos. Sci.* **40**, 2331–2343 (2023).
46. M. Watts, W. Maslowski, Y. J. Lee, J. C. Kinney, R. Osinski, A spatial evaluation of Arctic Sea Ice and regional limitations in CMIP6 historical simulations. *J. Climate* **34**, 6399–6420 (2021).
47. J. A. Screen, I. Simmonds, The central role of diminishing sea ice in recent Arctic temperature amplification. *Nature* **464**, 1334–1337 (2010).
48. W. Ma, H. Wang, G. Chen, L. R. Leung, J. Lu, P. J. Rasch, Q. Fu, B. Kravitz, Y. Zou, J. J. Cassano, W. Maslowski, The role of interdecadal climate oscillations in driving Arctic atmospheric river trends. *Nat. Commun.* **15**, 2135 (2024).
49. Z. Cai, Q. You, H. W. Chen, R. Zhang, D. Chen, J. Chen, S. Kang, J. Cohen, Amplified wintertime Barents Sea warming linked to intensified Barents oscillation. *Environ. Res. Lett.* **17**, 044068 (2022).
50. R. Knutti, M. A. A. Rugenstein, G. C. Hegerl, Beyond equilibrium climate sensitivity. *Nat. Geosci.* **10**, 727–736 (2017).
51. P. A. Stott, J. A. Kettleborough, Origins and estimates of uncertainty in predictions of twenty-first century temperature rise. *Nature* **416**, 723–726 (2002).
52. X. Chen, A. Dai, Quantifying contributions of external forcing and internal variability to Arctic warming during 1900–2021. *Earth's Future* **12**, e2023EF003734 (2024).
53. A. Dai, D. Luo, M. Song, J. Liu, Arctic amplification is caused by sea-ice loss under increasing CO2. *Nat. Commun.* **10**, 121 (2019).
54. N. Scafetta, Advanced testing of low, medium, and high ECS CMIP6 GCM simulations versus ERA5-T2m. *Geophys. Res. Lett.* **49**, e2022GL097716 (2022).
55. J. Hwang, Y.-S. Choi, H. Su, J. H. Jiang, Invariability of Arctic top-of-atmosphere radiative response to surface temperature changes. *Earth Space Sci.* **7**, e2020EA001316 (2020).
56. E. Rosenblum, I. Eisenman, Sea Ice trends in climate models only accurate in runs with biased global warming. *J. Climate* **30**, 6265–6278 (2017).
57. J. Ono, M. Watanabe, Y. Komuro, H. Tatebe, M. Abe, Enhanced Arctic warming amplification revealed in a low-emission scenario. *Commun. Earth Environ.* **3**, 27 (2022).
58. J. Huang, T. Ou, D. Chen, Y. Luo, Z. Zhao, The amplified arctic warming in the recent decades may have been overestimated by CMIP5 models. *Geophys. Res. Lett.* **46**, 13338–13345 (2019).
59. B. Y. Yim, H. S. Min, B.-M. Kim, J.-H. Jeong, J.-S. Kug, Sensitivity of Arctic warming to sea ice concentration. *Geophys. Res. Lett.* **121**, 6927–6942 (2016).
60. L. N. Boisvert, R. C. Boeke, P. C. Taylor, C. L. Parker, Constraining arctic climate projections of wintertime warming with surface turbulent flux observations and representation of surface-atmosphere coupling. *Front. Earth Sci.* **10**, 765304 (2022).
61. M. R. England, N. Feldl, Robust polar amplification in ice-free climates relies on ocean heat transport and cloud radiative effects. *J. Climate* **37**, 2179–2197 (2024).
62. C. W. Thackeray, A. Hall, An emergent constraint on future Arctic sea-ice albedo feedback. *Nat. Clim. Change* **9**, 972–978 (2019).
63. H. Hersbach, B. Bell, P. Berrisford, S. Hirahara, A. Horanyi, J. Munoz-Sabater, J. Nicolas, C. Peubey, R. Radu, D. Schepers, A. Simmons, C. Soci, S. Abdalla, X. Abellan, G. Balsamo, P. Bechtold, G. Biavati, J. Bidlot, M. Bonavita, G. De Chiara, P. Dahlgren, D. Dee, M. Diamantakis, R. Dragani, J. Flemming, R. Forbes, M. Fuentes, A. Geer, L. Haimberger, S. Healy, R. J. Hogan, E. Holm, M. Janiskova, S. Keeley, P. Laloyaux, P. Lopez, C. Lupu, G. Radnoti, P. de Rosnay, I. Rozum, F. Vamborg, S. Villaume, J. N. Thepaut, The ERA5 global reanalysis. *Quart. J. R. Meteor. Soc.* **146**, 1999–2049 (2020).
64. N. A. Rayner, D. E. Parker, E. B. Horton, C. K. Folland, L. V. Alexander, D. P. Rowell, E. C. Kent, A. Kaplan, Global analyses of sea surface temperature, sea ice, and night marine air temperature since the late nineteenth century. *J. Geophys. Res. Atmos.* **108**, 4407 (2003).
65. C. P. Morice, J. J. Kennedy, N. A. Rayner, J. P. Winn, E. Hogan, R. E. Killick, R. J. H. Dunn, T. J. Osborn, P. D. Jones, I. R. Simpson, An updated assessment of near-surface temperature change from 1850: The HadCRUT5 data set. *J. Geophys. Res. Atmos.* **126**, e2019JD032361 (2021).
66. N. J. L. Lenssen, G. A. Schmidt, J. E. Hansen, M. J. Menne, A. Persin, R. Ruedy, D. Zyss, Improvements in the GISTEMP uncertainty model. *J. Geophys. Res. Atmos.* **124**, 6307–6326 (2019).
67. R. A. Rohde, Z. Hausfather, The berkeley earth land/ocean temperature record. *Earth Syst. Sci. Data* **12**, 3469–3479 (2020).

68. V. Eyring, S. Bony, G. A. Meehl, C. A. Senior, B. Stevens, R. J. Stouffer, K. E. Taylor, Overview of the Coupled Model Intercomparison Project Phase 6 (CMIP6) experimental design and organization. *Geosci. Model Dev.* **9**, 1937–1958 (2016).

Acknowledgments: We appreciate the valuable comments and suggestions provided by the editors and reviewers. We also thank Fudan University and the University of Exeter for providing the computing platforms. **Funding:** Q.Y. is supported by the National Key Research and Development Program of China (2023YFE0123800 and 2022YFF0801703) and the Shanghai Pilot Program for Basic Research-Fudan University (grant no. 22TQ007). Z.C is supported by the China Scholarship Council (grant 202306100245). J.C is supported by the NSF grants AGS-2140909 and ARCSS-2115072. H.W.C is supported by the Strategic Research Area "ModElling the Regional and Global Earth system," MERGE, funded by the Swedish government, and the Hasselblad Foundation. **Author contributions:** Conceptualization: Z.C., Q.Y., J.A.S., Ru.Z., D.C., and J.C. Methodology: Q.Y., J.A.S., and J.C. Validation: Q.Y., Ru.Z., D.C., Re.Z., and J.C. Formal analysis: Z.C., Q.Y., and J.C. Resources: Ru.Z. Investigation: Q.Y., Ru.Z., and J.C. Writing—original draft: Z.C. and J.C. Writing—review and editing: Z.C., Q.Y., J.A.S., H.W.C., D.C., Ru.Z., Z.Z., J.C., Re.Z., and S.K. Visualization: Z.C., Q.Y., and J.C. Supervision: Q.Y., J.A.S., Ru.Z., and D.C. Project administration: Q.Y. Funding acquisition: Q.Y. **Competing interests:** The authors declare that they have no competing interests. **Data and materials availability:** The CMIP6 outputs (*68*) are available at https://aims2.llnl.gov/search/cmip6/. The ERA5 reanalysis dataset (*63*) is available at https://climate.copernicus.eu/climate-reanalysis. For the observational datasets, HadCRUT5 (*65*) is available at https://metoffice.gov.uk/hadobs/hadcrut5/. GISTEMP4 (*66*) is available at https://data.giss.nasa.gov/gistemp/, and BEST (*67*) is available at http://berkeleyearth.org/data/. The sea ice data are available from https://metoffice.gov.uk/hadobs/hadisst/ (*64*). All other data needed to evaluate the conclusions in the paper are present in the paper and/or the Supplementary Materials.

Submitted 11 July 2024
Accepted 31 January 2025
Published 5 March 2025
10.1126/sciadv.adr6413